Deep Learning Approaches for Teleseismic Discrimination and its Societal Implications

Rayna Arora[1] , **Ronan Le Bras**[2]
[1]CTBTO Youth Group
[2]CTBTO
rayna.aro@gmail.com, ronan.lebras@ctbto.org,

Abstract

The discrimination problem in seismology, i.e. the classification of seismic waves as originating from an explosion versus a tectonic event, has important implications for the safety and security of humankind. Although this problem has been well studied for decades and research in this area has been updated to take advantage of advances in Deep Learning, there still remains a critical gap in our knowledge. Previous research has only attempted to classify seismic waves at distances up to 400 km. We are extending this research to teleseismic distances, i.e. distances over 20 degrees or 2000 km. In this work we discuss the societal implications of accurate discrimination based solely on detections at these distances, and provide an approach to address this important problem. Our work builds on recent Deep Learning methods applied to various related tasks in seismology. We use hyperparameter tuning methods to considerably simplify some of the existing architectures that have been previously proposed, and demonstrate that it generalizes well. Our proposed model obtains competitive performance on the task of discriminating between explosions and tectonic events and performs much better on explosive rock burst events which were not used in training. All of our data has been assembled from public sources, and we provide this data as well as the related code in an open source repository.

1 Introduction

An accurate catalog of seismic events from tectonic sources is required for probabilistic seismic hazard analysis [McGuire, 2008]. Such hazard analysis is the basis for building codes that help determine the safety of human occupants as well as critical infrastructure. A common problem with seismic catalogs is the proliferation of mining activity that gets inadvertently captured and contaminates the catalog as noted by [Mackey *et al.*, 2003], for example. Consequently, an important post-processing step after the creation of a catalog is to classify the explosion events, and to remove them from the bulletin. This task of classifying an event as an explosion versus a natural tectonic event, or earthquake, is known as the *discrimination* problem in seismology.

Another important application of this discrimination task is for monitoring compliance with treaties banning nuclear testing. In the last century, the major nuclear powers signed various treaties limiting the size and number of nuclear tests that they could conduct. These limits were introduced to curb the development of increasingly lethal weapons which have endangered our existence as a species as well as to protect earth's ecosystems from the effects of the radiation released by these tests. These efforts to rein in nuclear testing culminated in the Comprehensive Nuclear-Test-Ban Treaty[UN, 1996], which bans all nuclear testing anywhere on earth, and has been signed by 185 countries.

While earthquakes and explosions can both generate a vast amount of energy, the forces involved are very different. Explosions release energy in a small volume around the source, and this causes mostly compressional waves, or P phases, to radiate outwards homogeneously. Earthquakes, on the other hand, release energy over multiple kilometers along a fault line and mostly in the form of shear waves, or S phases, that could have an asymmetric radiation pattern. These differences show up in the waveforms that are detected at seismic stations, and form the basis of work on discrimination.

At distances less than 2000 km, a number of seismic *phases*[Bormann *et al.*, 2013], each of which corresponds to a distinct wave path through the Earth, are normally detected. Many methods rely on contrasting the detections of multiple phases from the same event. For example, the spectral characteristics of the P versus the L_g phase (a type of surface wave that can be detected up to a few hundred kilometers) are an easy marker for discrimination purposes as shown in [Dysart and Pulli, 1990]. At teleseismic distances, however, it is unusual to detect anything except a P phase.

There are some unfortunate ramifications of having good discrimination methods that only work well at short distances. The main issue is that these methods can only be applied to events that occur in regions of the earth that are covered with very dense seismic networks. In other words, if a country wishes to use the latest techniques for seismic hazard analysis it must have the resources to deploy and maintain many stations. This creates an inequity in preparedness which causes poorer countries to be affected significantly more by natural disasters than richer countries. [Nairobi, 2005].

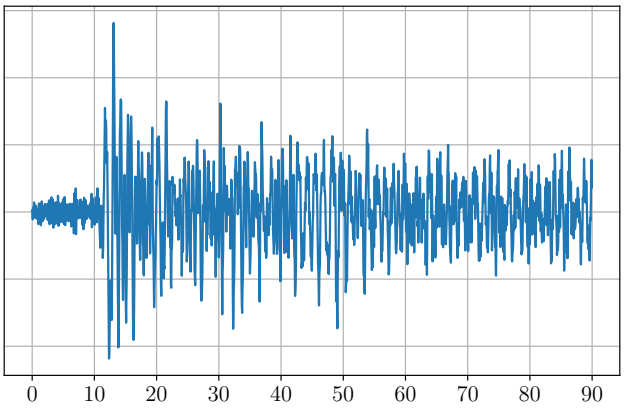

Figure 1: An earthquake of magnitude 6.1 mb detected at 86.09 degrees distance. (90 seconds snippet with onset at 10 seconds)

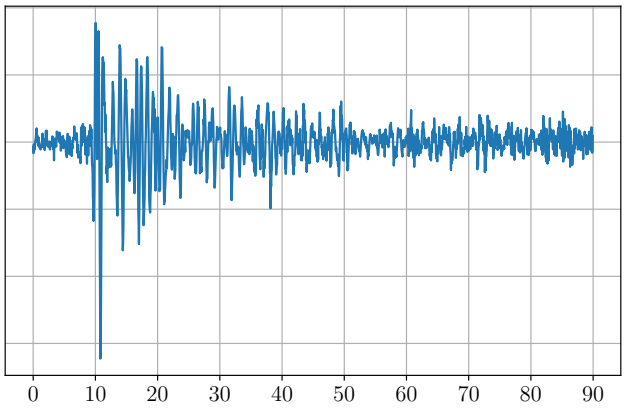

Figure 2: An explosion of magnitude 6.3 mb detected at 91.02 degrees distance. (90 seconds snippet with onset at 10 seconds)

For the purpose of monitoring compliance with a global treaty such as the CTBT, these regional discrimination methods have limited utility. The CTBTO's network of seismic stations maintained by the IMS (International Monitoring System) is too sparse to provide an assurance that a nuclear explosion test will be detected by at least one of the stations within 200 km. For example, [Stump *et al.*, 2002] has done an analysis of the IMS network when it is fully operational. This work shows that 90% of the earth's land mass will be covered by at least one station within 2000 km, but only 10% is within 200 km of an IMS station. Of course, member states that have signed the CTBT are free to use data obtained from other seismic networks to make their own determination as to the source of an event. However, there is no guarantee that such additional data will be available for all regions of the world. This brings into question the ability of the treaty to be effectively monitored. Given that the US Senate has refused to ratify the treaty citing concerns of monitoring capability [Pifer, 2016], it is important to address these concerns for the ultimate safety of the earth's population from further development of atomic weapons.

For the above reasons, our work aims to extend the capabilities of existing discrimination methods. Although it is much harder to accurately classify seismic waveforms at distances over 2000 km, we note that it is not entirely intractable. For example, we show waveforms in Figures 1 and 2 from an earthquake and an explosion respectively detected at teleseismic distances. In this example, the impulsive nature of the explosion event shows up in the sharp onset spike visible in the waveform. Of course, for smaller magnitude events such clear features are not immediately obvious.

In the rest of this paper we describe the methods that have been applied to this problem, which are almost exclusively designed for regional distances, as well as our methodology for adapting these methods, and our data gathering techniques and experimental results.

2 Related Work

The importance of discrimination between earthquakes and explosions for the purpose of seismic hazard analysis as well as nuclear explosion monitoring is well documented in the literature. We refer the reader to [Rabin *et al.*, 2016] for a good overview of this topic. As mentioned in the paper, many of the previously developed methods rely on computing parameters computed from input waveforms such as event magnitude. Further, these parametric methods often require the detection of different types of seismic phases to be used for discrimination. For example, the Ms:mb ratio method [Blandford, 1982] requires the detection of a surface wave and a body wave in order to compute two different magnitude estimates. The limitation of such methods for a global seismic network are apparent in the statistics. [Rabin *et al.*, 2016] goes on to report that such parametric methods are only applicable to 60% of all events reported by the CTBTO in years 2011-2013.

In recent years, the focus has shifted to applying Deep Learning directly on spectrograms for the purpose of discrimination, for example [Magana-Zook and Ruppert, 2017]. Also, in [Linville *et al.*, 2019] the authors show results on architectures based on Convolutional Neural Nets (CNNs) as well as Long Short-term Memory (LSTM). We show these architectures in Figures 3 and 4 respectively. Although these architectures have only been tested for discrimination at regional distances, we believe that these can be adapted to teleseismic distances since they require nothing more than a spectrogram of the waveform as an input. However, other approaches such as [Ranasinghe *et al.*, 2019], which are also based on CNNs, but require both a P and an S phase to be detected are not as easy to use since S phases are rarely detected at higher distances. Similarly, approaches based on Support Vector Machines such as [Kim *et al.*, 2020] that require features from both P and S phases are inapplicable for teleseismic discrimination.

We note that there are a number of methods based on waveforms that we could extend to teleseismic distances such as [Pezzo *et al.*, 2003], [Li *et al.*, 2018], [Ross *et al.*, 2018],

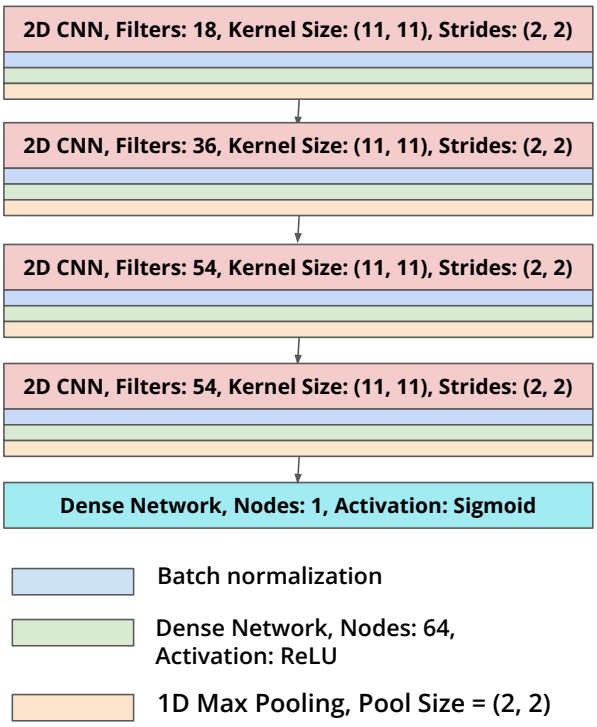

Figure 3: Linville et al. CNN.

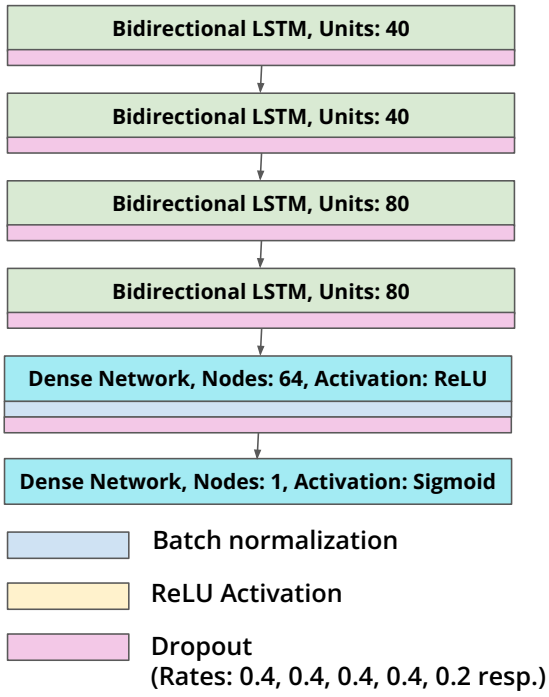

Figure 4: Linville et al. LSTM.

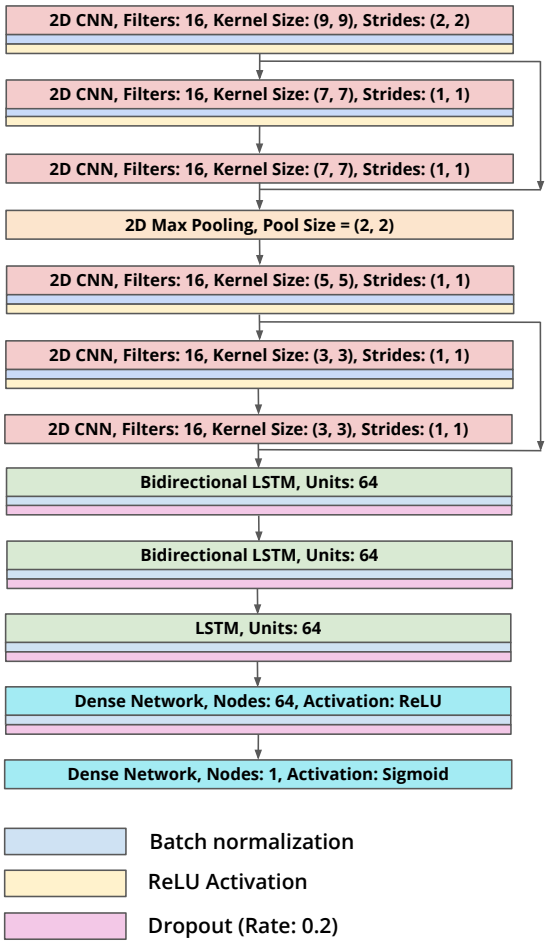

Figure 5: CRED Architecture (Mousavi et al.).

[Miao *et al.*, 2020], [Wei *et al.*, 2020], or [Ray *et al.*, 2017]. All of them are designed to solve various classification tasks in seismology without any assumptions on explicit feature extraction. In this paper we focus on Cnn-Rnn Earthquake Detector (CRED) [Mousavi *et al.*, 2019] since its architectures is the most versatile. As shown in Figure 5, it uses a mix of convolutional and recurrent layers in a residual structure. CRED was proposed to discriminate seismic phases from noise, but there is no reason it can't be used for other classification tasks. Similar to most other models it uses the spectrograms of the waveforms as input, and has only been tested on regional detections.

3 Data

There is no existing dataset for teleseismic discrimination, so as part of our work we had to build one. We collected seismic event data from the online bulletins published by the International Seismic Centre (ISC)[Storchak *et al.*, 2017; Storchak *et al.*, 2020] and corresponding waveforms from the waveform repository published by the Incorporated Research Institutions for Seismology (IRIS).

The ISC event bulletins have an optional field describing

the source of each event. For a small subset of these events this field is filled in with either earthquake, explosion, or rockburst[Lu *et al.*, 2013]. We selected all the events with these three possible sources and then used the IRIS waveform repository to obtain the waveforms from stations which had detected the event according to the bulletin. However, some waveforms didn't show any clear signal and had to be discarded. We used the STA/LTA (short-term average divided by the long-term average) method [Allen, 1978] to determine if there was a suitable detection in the waveform. For each valid waveform, we kept 90 seconds of data; 10 seconds before the onset and 80 seconds after the onset. This waveform snippet was high-pass filtered at 1 Hz and normalized. We only kept the waveform corresponding to the vertical channel and downsampled it to 20 samples per second.

The following steps describe the overall data gathering procedure.

- For each ISC event bulletin from 1970 to 2018:
  - For each event in bulletin, if event source is either earthquake, explosion, or rockburst:
    - For each station at a distance of 20 degrees or more that detects the event:
      1. Download a waveform snippet around the onset time.
      2. High-pass filter at 1 Hz.
      3. If the STA/LTA reaches or exceeds 2 within 5 seconds of onset time:
         - Add this waveform to the dataset. Record the event parameters and distance of station to event.

Since the earthquake data far exceeds the explosion data, we used stratified sampling of the earthquake waveforms to ensure that the number of earthquakes and explosions in each distance bucket from 20 to 180 degrees in steps of 10 degrees are balanced.

In total, we have 7608 data points. All of our data is available in an open source repository https://github.com/RaynaArora/TeleseismicDiscrimination/tree/main/ijcai2021.

4 Methods

In our work, we use the CRED architecture as a basis. However, instead of using a spectrogram of the waveform as input we found the performance to be better by using the waveforms directly. We also made a number of other simplifications to the model by systematically identifying the best architecture. We used grid search to tune the following hyperparameters on the validation data:

1. The kernel size in each convolutional layer, varied from 10 to 40 in steps of 2.
2. The number of filters in each convolutional layer, varied from 16 to 320 in steps of 16.
3. The units (output dimension) in each LSTM or Bidirectional LSTM layer, varied from 32 to 128 in steps of 32.
4. The number of convolutional, LSTM, and Bidirectional LSTM layers, varied from 1 to 5 in steps of 1.

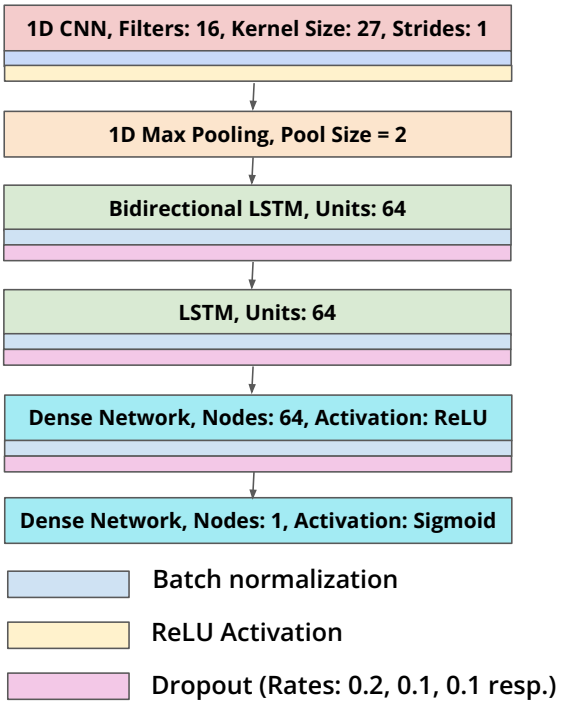

Figure 6: Our architecture.

5. Whether or not to use a residual layer (only when considering more than one convolutional layer).
6. The dropout rates in the LSTM and dense layers, varied from 0.1 to 0.4 in steps of 0.1.
7. The number of nodes in the dense layer — 64 or 128.
8. Whether to use a spectrogram or waveform as input.

The resulting optimal architecture is described in Figure 6.

5 Experiments

We used the Keras software package with the Adam optimizer for training all the Deep Learning architectures that we evaluated. In our experiments we divided the data into 80% training, 10% validation, and 10% test. All the hyperparameters were tuned on the validation set. The models were trained with a batch size of 32 and training was stopped when the validation accuracy plateaued for 60 epochs. The training time on a p2.xlarge instance on AWS was roughly 60 minutes.

Table 1 shows the results of our architecture as well as 3 other architectures in the literature. Our model and CRED achieve very similar accuracies. However, our method gets the highest Area Under the Curve (AUC) and has the least number of parameters by a factor of 2. The ROC curve is shown in Figure 7.

Figure 8 shows our model's accuracy versus distance detected. This graph demonstrates that our model generalizes well across all distances. We also plot the accuracy of our model by event magnitude in Figure 9. Our accuracy is quite low in the 3 to 3.5 range, which comprises less than 1% of

Model	Accuracy	AUC	Parameters
Proposed Method	89.5 %	0.962	96,641
Mousavi et al. (CRED)	89.7 %	0.957	208,273
Linville et al. CNN	83.9 %	0.896	456,237
Linville et al. RNN	80.9 %	0.894	375,425

Table 1: Comparison of 4 models

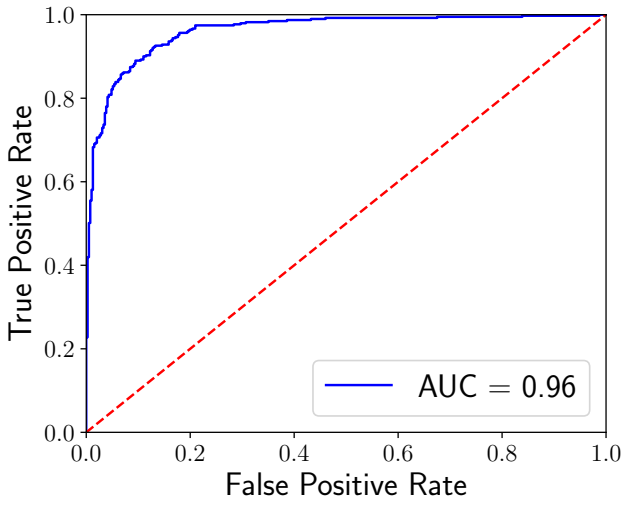

Figure 7: Receiver Operating Characteristic curve for proposed method. AUC (Area Under the Curve) is 0.96.

our data, and hence we have insufficient samples to train or evaluate. On the other hand, our accuracy of 90% in the 3.5 to 4.0 mb range is very promising because this range is critical for treaty monitoring purposes. Finally, in Figure 10 we show the accuracy numbers of our model as a function of the maximum STA/LTA value in a small window around the onset time of the detection. This graph shows that the accuracy of our model increases with STA/LTA. In other words, when the seismic waveform is much larger than the background noise levels it is easier to discriminate the source of the waveform.

In the above experiments, we trained and tested our models on data from explosions and earthquakes only. In order to test the generalization capability of our models, we tested all the models on novel rockburst data. As explained in [Ma *et al.*, 2015]

> Rockburst is the sudden release of elastic strain energy in rock masses under high local stresses, as a result of rock fragmentation, ejection, projection and even earthquakes.

Rockbursts are similar to explosions in nature and we expect our models to classify them as such. As shown in Table 2, our model achieves the highest accuracy on this novel dataset.

6 Conclusion

We have demonstrated for the first time that it is possible to discriminate between earthquakes and explosions detected at teleseismic distances. Even with limited data we were able

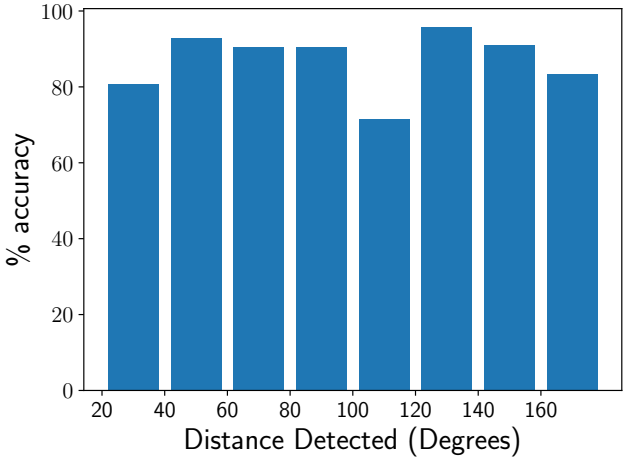

Figure 8: Accuracy by distance detected.

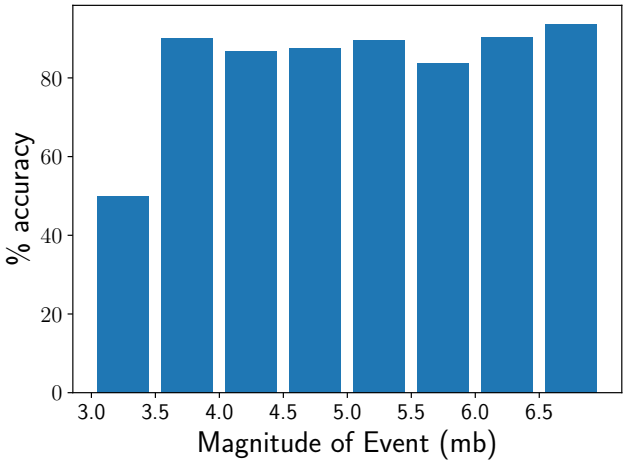

Figure 9: Accuracy by event magnitude.

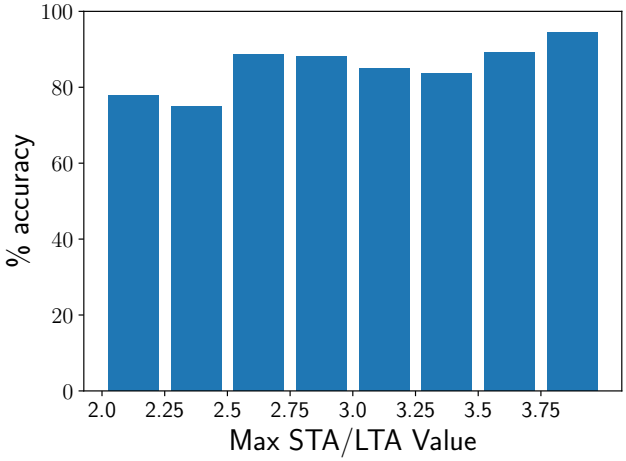

Figure 10: Accuracy by maximum STA/LTA value within 5 seconds of the detection onset time.

Model	Rockburst Accuracy
Proposed Method	96.7 %
Mousavi et al. (CRED)	94.6 %
Linville et al. CNN	95.2 %
Linville et al. RNN	82.1 %

Table 2: Comparison of rockburst accuracies

to achieve nearly 90% accuracy. Using seismic waveforms rather than spectrograms as inputs made it possible to train a model with far fewer parameters that generalized better for unseen inputs such as rockbursts.

We have taken an important step towards making treaty monitoring feasible from a sparse global seismic network. Furthermore, we expect that our work can be applied to improve seismic hazard analysis in developing nations with a sparse seismic network, thereby mitigating the disproportionate casualties counts these countries suffer due to earthquakes.

Acknowledgements

The views expressed herein are those of the author(s) and do not necessarily reflect the views of the CTBTO Preparatory Commission.

Dr. Nimar S. Arora provided valuable guidance on the general direction of this project.

The facilities of IRIS Data Services, and specifically the IRIS Data Management Center, were used for access to waveforms, related metadata, and/or derived products used in this study. IRIS Data Services are funded through the Seismological Facilities for the Advancement of Geoscience (SAGE) Award of the National Science Foundation under Cooperative Support Agreement EAR-1851048.

All seismic data were downloaded through the IRIS Wilber 3 system https://ds.iris.edu/wilber3/ or IRIS Web Services https://service.iris.edu/, including the following seismic networks: (1) the AZ (ANZA; UC San Diego, 1982); (2) the TA (Transportable Array; IRIS, 2003); (3) the US (USNSN, Albuquerque, 1990); (4) the IU (GSN; Albuquerque, 1988).

References

[Allen, 1978] Rex V Allen. Automatic earthquake recognition and timing from single traces. *Bulletin of the Seismological Society of America*, 68(5):1521–1532, 1978.

[Blandford, 1982] Robert R Blandford. Seismic event discrimination. *Bulletin of the Seismological Society of America*, 72(6B):S69–S87, 1982.

[Bormann *et al.*, 2013] Peter Bormann, Dmitry A Storchak, and Johannes Schweitzer. The iaspei standard nomenclature of seismic phases. In *New Manual of Seismological Observatory Practice 2 (NMSOP-2)*, pages 1–20. Deutsches GeoForschungsZentrum GFZ, 2013.

[Dysart and Pulli, 1990] Paul S Dysart and Jay J Pulli. Regional seismic event classification at the noress array: seismological measurements and the use of trained neural networks. *Bulletin of the Seismological Society of America*, 80(6B):1910–1933, 1990.

[Kim *et al.*, 2020] Sangkyeum Kim, Kyunghyun Lee, and Kwanho You. Seismic discrimination between earthquakes and explosions using support vector machine. *Sensors*, 20(7):1879, Mar 2020.

[Li *et al.*, 2018] Zefeng Li, Men-Andrin Meier, Egill Hauksson, Zhongwen Zhan, and Jennifer Andrews. Machine learning seismic wave discrimination: Application to earthquake early warning. *Geophysical Research Letters*, 45(10):4773–4779, May 2018.

[Linville *et al.*, 2019] Lisa Linville, Kristine Pankow, and Timothy Draelos. Deep learning models augment analyst decisions for event discrimination. *Geophysical Research Letters*, 46(7):3643–3651, Feb 2019.

[Lu *et al.*, 2013] Cai-Ping Lu, Lin-Ming Dou, Nong Zhang, Jun-Hua Xue, Xiao-Nan Wang, Hui Liu, and Jun-Wei Zhang. Microseismic frequency-spectrum evolutionary rule of rockburst triggered by roof fall. *International Journal of Rock Mechanics and Mining Sciences*, 64:6–16, 2013.

[Ma *et al.*, 2015] T.H. Ma, C.A. Tang, L.X. Tang, W.D. Zhang, and L. Wang. Rockburst characteristics and microseismic monitoring of deep-buried tunnels for jinping ii hydropower station. *Tunnelling and Underground Space Technology*, 49:345–368, 2015.

[Mackey *et al.*, 2003] Kevin G. Mackey, Kazuya Fujita, Larissa V. Gounbina, Boris M. Koz'min, Valery S. Imaev, Ludmilla P. Imaeva, and Boris M. Sedov. Explosion contamination of the northeast siberian seismicity catalog: Implications for natural earthquake distributions and the location of the tanlu fault in Russia. *Bulletin of the Seismological Society of America*, 93(2):737–746, 04 2003.

[Magana-Zook and Ruppert, 2017] S. A. Magana-Zook and S. D. Ruppert. Explosion Monitoring with Machine Learning: A LSTM Approach to Seismic Event Discrimination. In *AGU Fall Meeting Abstracts*, volume 2017, pages S43A–0834, December 2017.

[McGuire, 2008] Robin K McGuire. Probabilistic seismic hazard analysis: Early history. *Earthquake Engineering & Structural Dynamics*, 37(3):329–338, 2008.

[Miao *et al.*, 2020] Fajun Miao, N. Seth Carpenter, Zhenming Wang, Andrew S. Holcomb, and Edward W. Woolery. High-accuracy discrimination of blasts and earthquakes using neural networks with multiwindow spectral data. *Seismological Research Letters*, 91(3):1646–1659, Mar 2020.

[Mousavi *et al.*, 2019] S. Mostafa Mousavi, Weiqiang Zhu, Yixiao Sheng, and Gregory C. Beroza. Cred: A deep residual network of convolutional and recurrent units for earthquake signal detection. *Scientific Reports*, 9(1), Jul 2019.

[Nairobi, 2005] Nairobi. Natural disasters —a heavy price to pay. *The New Humanitarian*, May 2005.

[Pezzo *et al.*, 2003] E. Del Pezzo, A. Esposito, M. Marinaro, M. Martini, and S. Scarpetta. Discrimination of

earthquakes and underwater explosions using neural networks. *Bulletin of the Seismological Society of America*, 93(1):215–223, Feb 2003.

[Pifer, 2016] Steven Pifer. What's the deal with senate republicans and the test ban treaty? *Brookings*, Sep 2016.

[Rabin *et al.*, 2016] Neta Rabin, Yuri Bregman, Ofir Lindenbaum, Yochai Ben-Horin, and A. Averbuch. Earthquake-explosion discrimination using diffusion maps. *Geophysical Journal International*, 207(3):1484–1492, Jun 2016.

[Ranasinghe *et al.*, 2019] N. R. Ranasinghe, L. Huang, T. Clee, and J. A. Kemp. A deep learning approach to discriminate between explosions and earthquakes. In *AGU Fall Meeting Abstracts*, volume 2019, pages S43D–0674, December 2019.

[Ray *et al.*, 2017] Jaideep Ray, Clifford Hansen, Robert Forrest, and Christopher J. Young. Using discrete wavelet transforms to discriminate between noise and phases in seismic waveforms., Apr 2017.

[Ross *et al.*, 2018] Zachary E. Ross, Men-Andrin Meier, Egill Hauksson, and Thomas H. Heaton. Generalized seismic phase detection with deep learning. *Bulletin of the Seismological Society of America*, 108(5A):2894–2901, Aug 2018.

[Storchak *et al.*, 2017] Dmitry A. Storchak, James Harris, Lonn Brown, Kathrin Lieser, Blessing Shumba, Rebecca Verney, Domenico Di Giacomo, and Edith I. M. Korger. Rebuild of the bulletin of the international seismological centre (ISC), part 1: 1964–1979. *Geoscience Letters*, 4, Dec 2017.

[Storchak *et al.*, 2020] Dmitry A. Storchak, James Harris, Lonn Brown, Kathrin Lieser, Blessing Shumba, and Domenico Di Giacomo. Rebuild of the bulletin of the international seismological centre (ISC)—part 2: 1980–2010. *Geoscience Letters*, 7, Nov 2020.

[Stump *et al.*, 2002] Brian W Stump, Michael AH Hedlin, D Craig Pearson, and Vindell Hsu. Characterization of mining explosions at regional distances: Implications with the international monitoring system. *Reviews of Geophysics*, 40(4):2–1, 2002.

[UN, 1996] UN. Comprehensive Nuclear-Test-Ban Treaty (CTBT). https://www.ctbto.org/the-treaty/treaty-text/, 1996. Accessed: 2021-5-10.

[Wei *et al.*, 2020] Hui Wei, Weiwei Shu, Longjun Dong, Zhongying Huang, and Daoyuan Sun. A waveform image method for discriminating micro-seismic events and blasts in underground mines. *Sensors*, 20(15):4322, Aug 2020.

A Kernel Activations

In this section we show the result of convolving the example earthquake and explosion from Figures 1 and 2, respectively, with the learned convolution kernels.

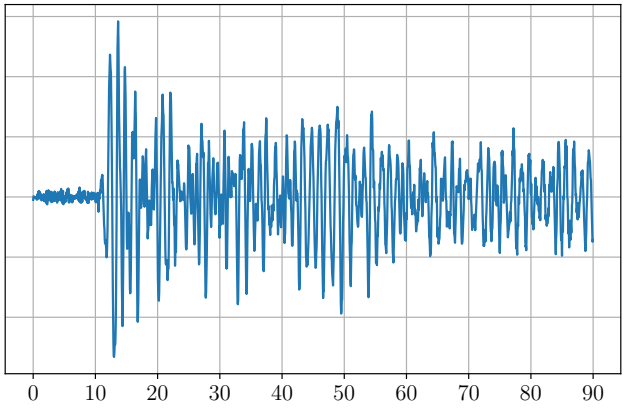

Figure 11: Example earthquake convolved with kernel 1.

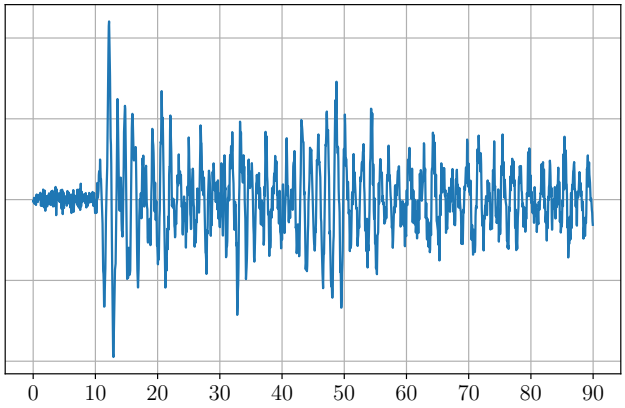

Figure 12: Example earthquake convolved with kernel 2.

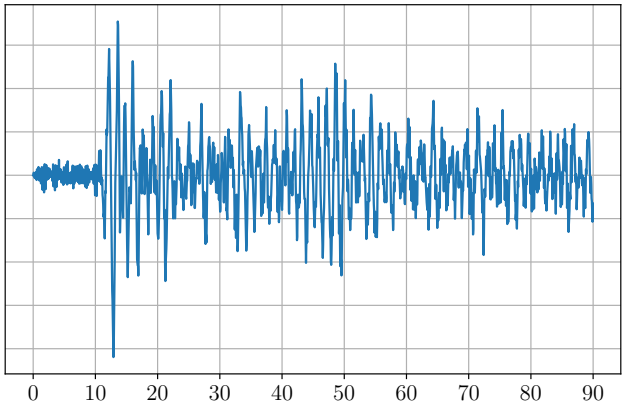

Figure 13: Example earthquake convolved with kernel 3.

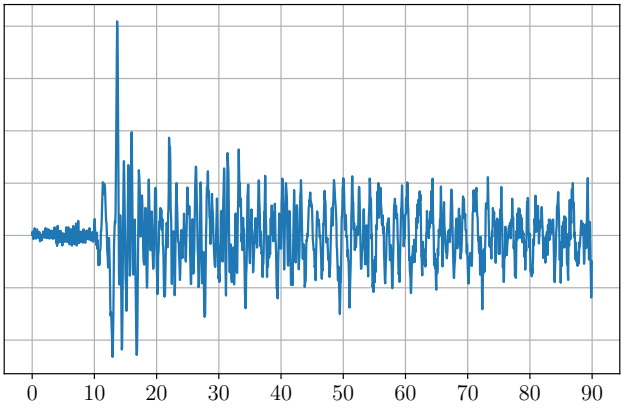

Figure 14: Example earthquake convolved with kernel 4.

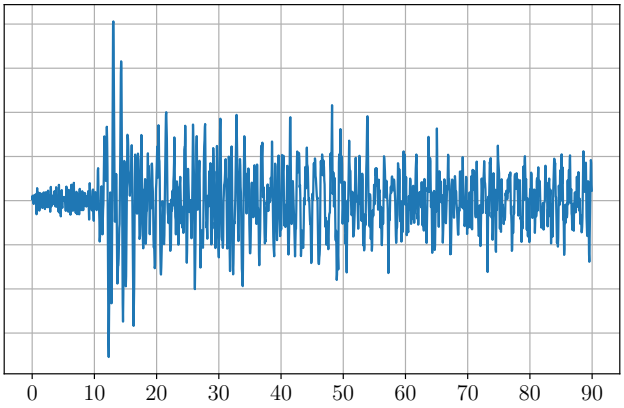

Figure 15: Example earthquake convolved with kernel 5.

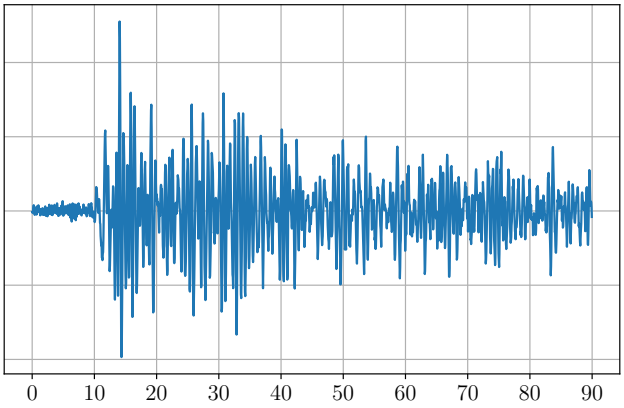

Figure 16: Example earthquake convolved with kernel 6.

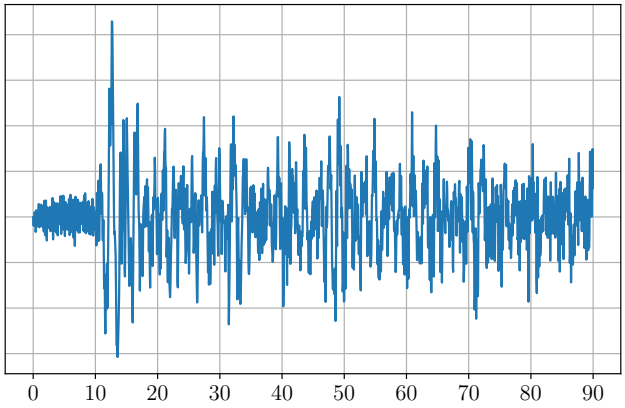

Figure 17: Example earthquake convolved with kernel 7.

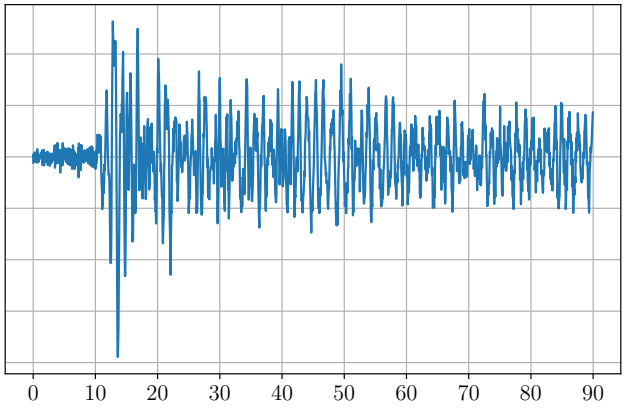

Figure 18: Example earthquake convolved with kernel 8.

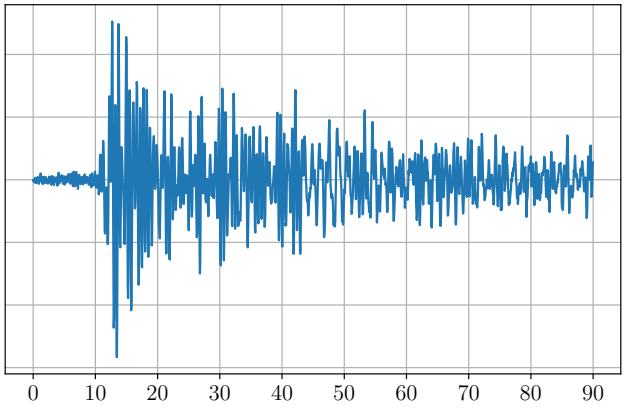

Figure 19: Example earthquake convolved with kernel 9.

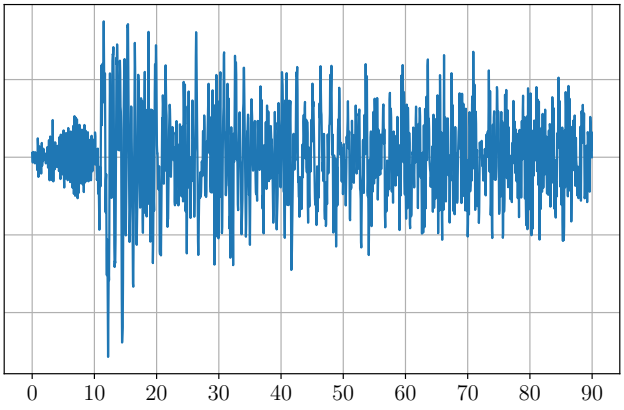

Figure 20: Example earthquake convolved with kernel 10.

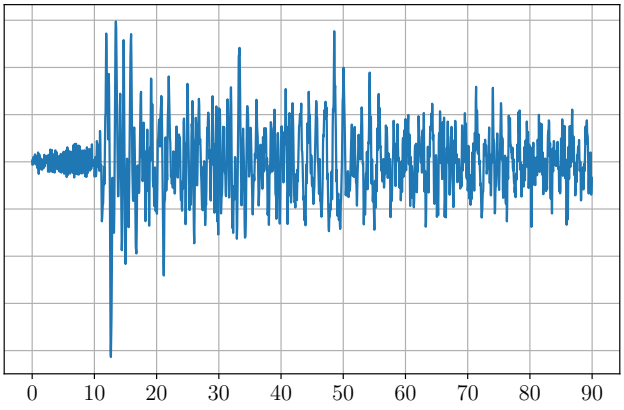

Figure 21: Example earthquake convolved with kernel 11.

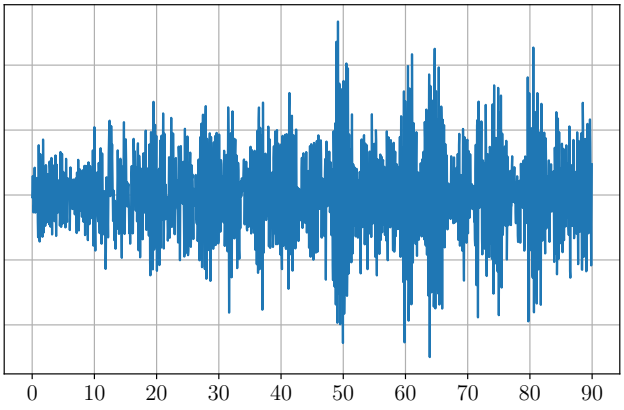

Figure 22: Example earthquake convolved with kernel 12.

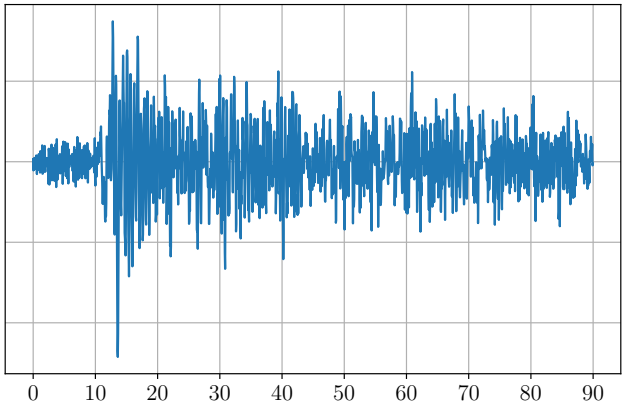

Figure 23: Example earthquake convolved with kernel 13.

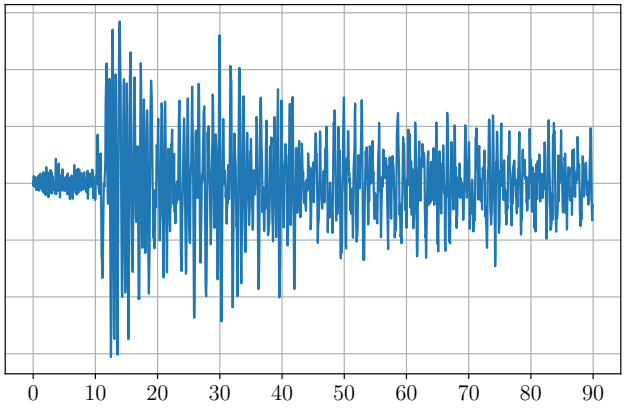

Figure 24: Example earthquake convolved with kernel 14.

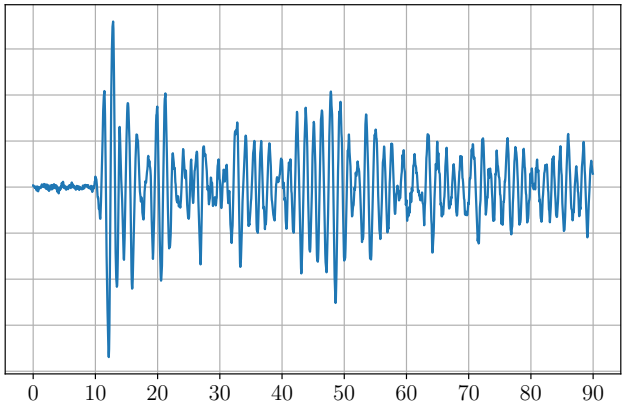

Figure 25: Example earthquake convolved with kernel 15.

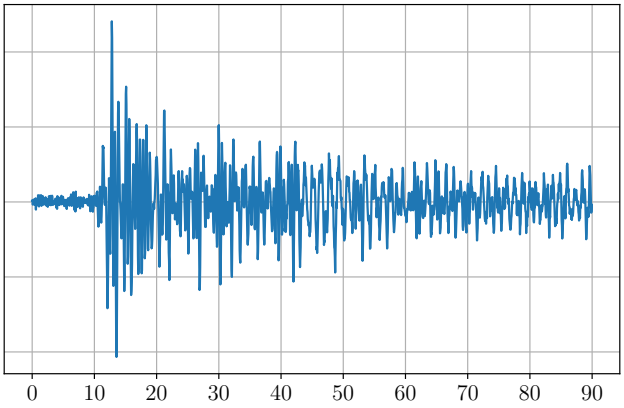

Figure 26: Example earthquake convolved with kernel 16.

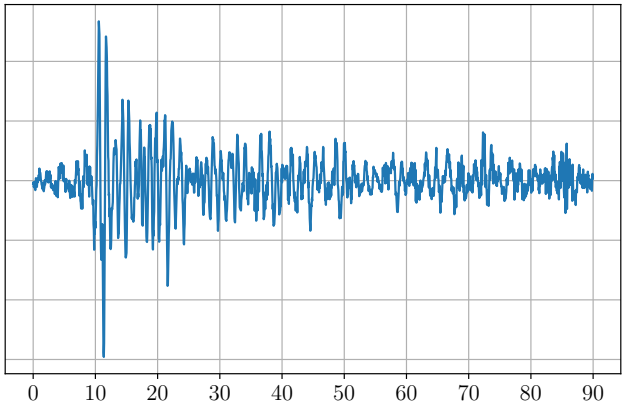

Figure 29: Example explosion convolved with kernel 3.

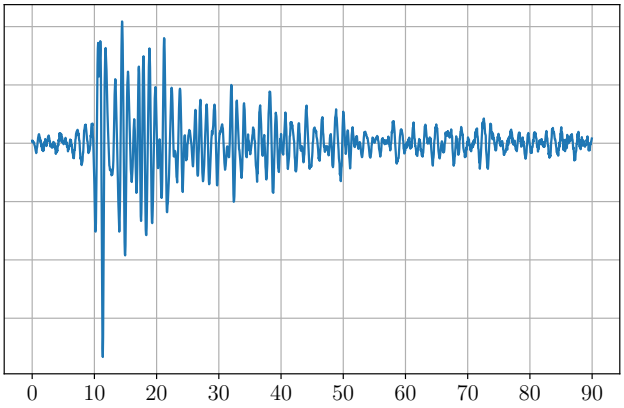

Figure 27: Example explosion convolved with kernel 1.

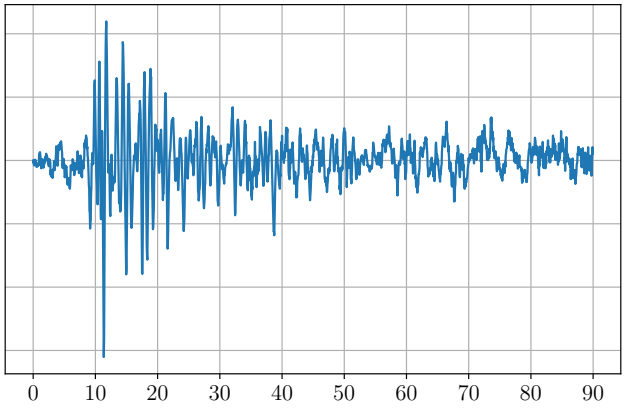

Figure 30: Example explosion convolved with kernel 4.

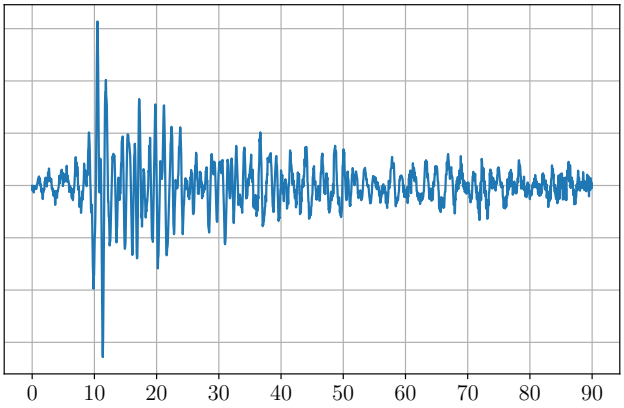

Figure 28: Example explosion convolved with kernel 2.

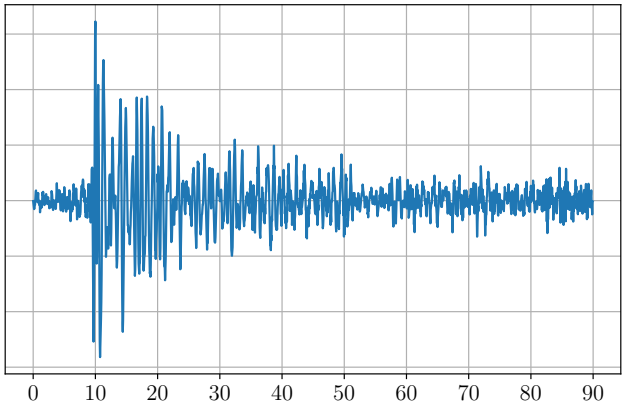

Figure 31: Example explosion convolved with kernel 5.

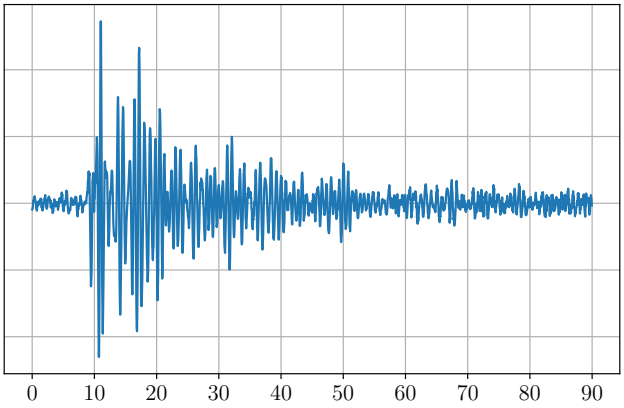

Figure 32: Example explosion convolved with kernel 6.

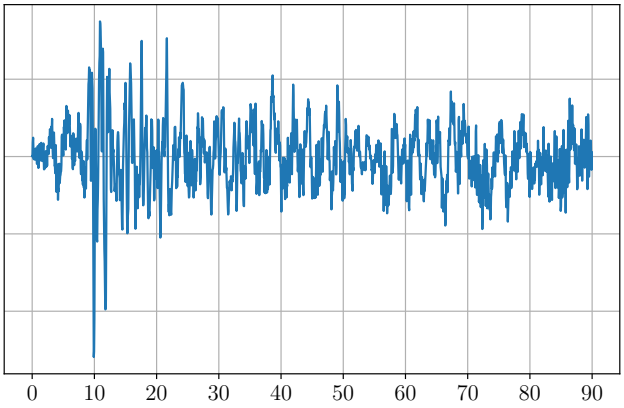

Figure 33: Example explosion convolved with kernel 7.

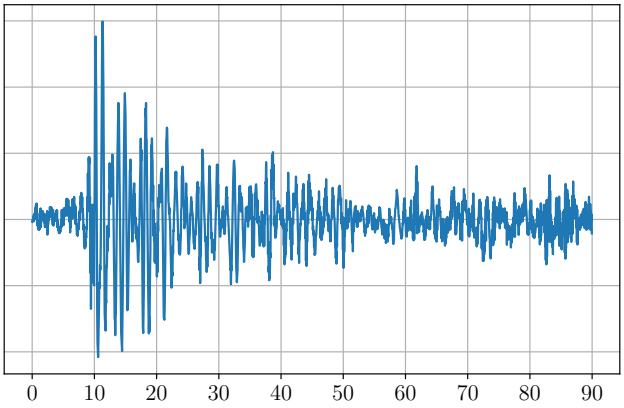

Figure 34: Example explosion convolved with kernel 8.

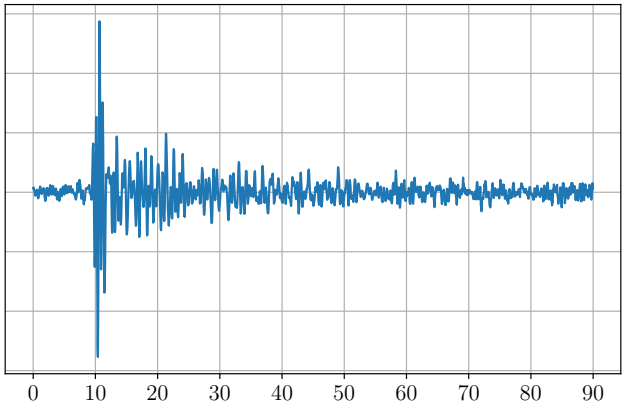

Figure 35: Example explosion convolved with kernel 9.

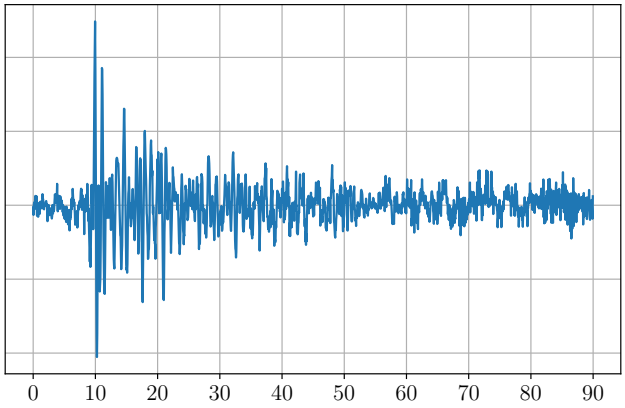

Figure 36: Example explosion convolved with kernel 10.

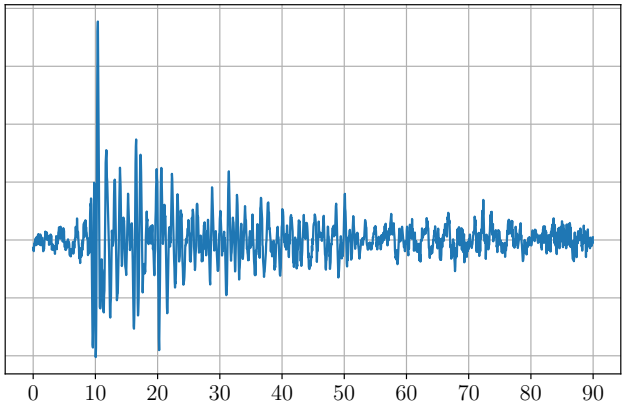

Figure 37: Example explosion convolved with kernel 11.

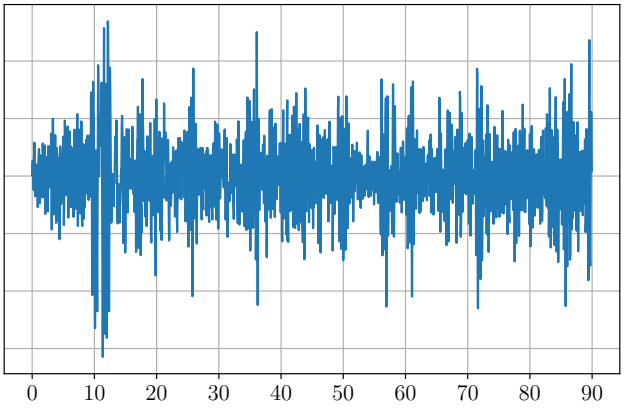

Figure 38: Example explosion convolved with kernel 12.

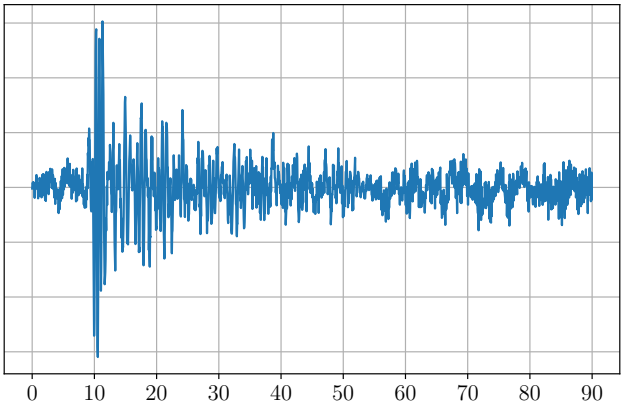

Figure 39: Example explosion convolved with kernel 13.

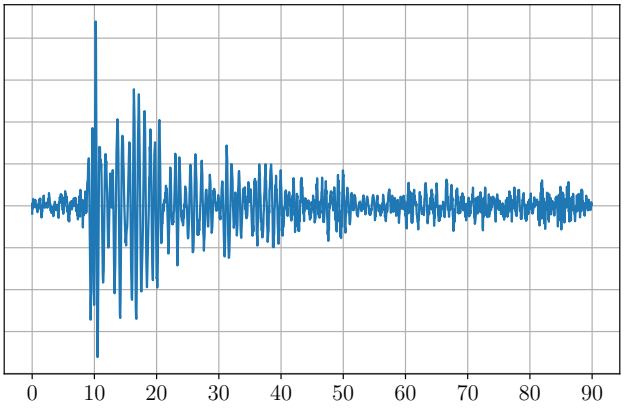

Figure 40: Example explosion convolved with kernel 14.

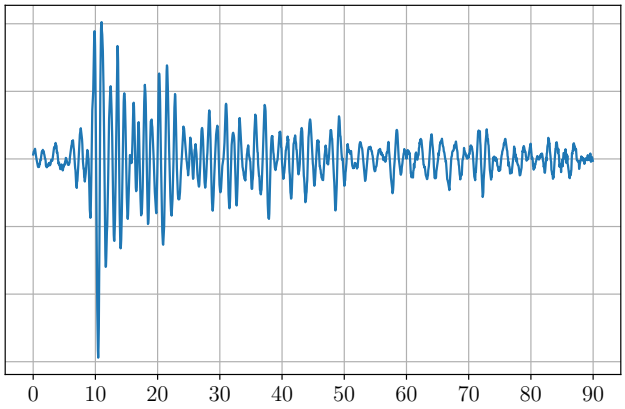

Figure 41: Example explosion convolved with kernel 15.

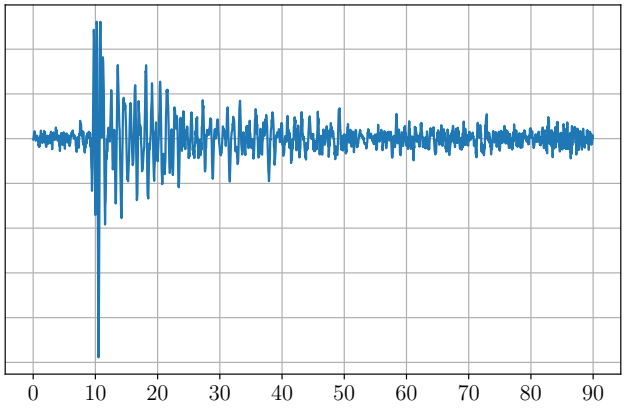

Figure 42: Example explosion convolved with kernel 16.